ACS APPLIED MATERIALS & INTERFACES

Research Article

www.acsami.org

# High-Value Utilization of Lignin to Synthesize Ag Nanoparticles with Detection Capacity For $Hg^{2+}$

Zuguang Shen,[†] Yuqiong Luo,[†] Qun Wang,[‡] Xiaoying Wang,*[,†] and Runcang Sun[†,§]

[†]State Key Laboratory of Pulp & Paper Engineering, South China University of Technology, Guangzhou 510640, China

[‡]Department of Chemical and Biological Engineering, Iowa State University, Ames, Iowa 50011, United States

[§]China Beijing Key Laboratory of Lignocellulosic Chemistry, Beijing Forestry University, Beijing 100083, China

**ABSTRACT:** This study reports the rapid preparation of silver nanoparticles (AgNPs) from Tollens' reagent under microwave irradiation. In the synthesis, lignin with reducing groups and spatial three-dimensional structure was used as reducing and stabilizing agents without other chemical reagents, and the effects of the ratio of lignin to $Ag^+$, reaction temperature, and heating time on the synthesis of AgNPs were investigated. The obtained AgNPs were further characterized by UV−vis, Malvern particle size, TEM, XRD, and XPS analyses. The structural changes of lignin before and after reaction were also studied by FT-IR, $^1$H NMR, $^{13}$C NMR, and GC−MS. The results revealed that the obtained AgNPs were mostly spherical with diameters of around 24 nm. The optimum reaction conditions were a ratio 50 mg of lignin to 0.3 mM of $Ag^+$, a microwave irradiation temperature of 60 °C, and a heating time of 10 min. Moreover, AgNPs redispersed well in water and ethanol after centrifugation for the removal of lignin. During the formation of AgNPs, lignin was oxidized, and the side chains of lignin were partly disrupted into small molecules, such as hydrocarbon and alcohol. The resultant lignin−AgNPs showed highly selective sensing detection for $Hg^{2+}$, and the color of the lignin−AgNP solution containing $Hg^{2+}$ decreased gradually with increasing amounts of $Hg^{2+}$ within seconds, but the other 19 metal ions had little effect on the color and surface plasmon absorption band of the lignin−AgNPs. Also, there was a linear relationship between the absorbance and $Hg^{2+}$ concentration, with a limit of detection concentration of 23 nM. This study provides not only a new way to take advantage of agricultural and forestry residues, but also a green and rapid method for the synthesis of AgNPs to detect the toxic ion $Hg^{2+}$ selectively and sensitively.

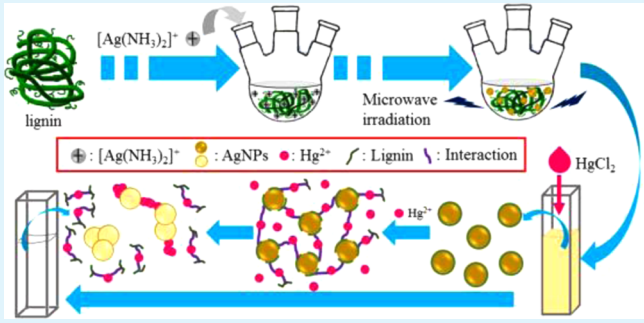


**KEYWORDS:** *Ag nanoparticles, lignin, microwave irradiation, high selectivity and sensitivity, high-value utilization*

## 1. INTRODUCTION

Recently, selective and sensitive chemosensors have been widely used in the detection of $Hg^{2+}$,[1,2] which is a highly toxic metal ion and has many harmful effects on humans and the environment. Among these sensors, noble metal gold nanoparticles (AuNPs) and silver nanoparticles (AgNPs) have attracted great attention as colorimetric probes, which can enable the direct detection of analytes through the monitoring of color changes with the naked eye as well as fluorescent and UV−vis spectroscopy. Recently, more and more research about AgNPs was reported. Sun et al. detected $Hg^{2+}$ in blood and wastewater with AgNPs.[3] Duan et al. have reported an investigation of a facile colorimetric sensor for $Hg^{2+}$ in aqueous solution based on the antiaggregation of AgNPs.[4] Rastogi et al. reported a highly sensitive and selective method for the colorimetric detection of $Hg^{2+}$ in an aqueous system by using label-free AgNPs.[5] The color change of AgNPs relates to the surface plasmon absorption band, which is dependent on many parameters such as the size, shape, capping agent, medium refractive index, and state of AgNPs.[6] Therefore, it is important to find a way to synthesize suitable AgNPs.

With the development of nanotechnology, many approaches have been used for the synthesis of AgNPs, including UV irradiation reduction, $\gamma$ irradiation, thermal decomposition, chemical reduction, and laser irradiation.[7−11] Chemical reduction method is one of the most commonly used methods. However, many chemical reduction methods require reducing agents like sodium borohydride and hydrazine hydrate and stabilizing agents like sodium citrate and surfactant, and all are harmful to environment. Furthermore, it is difficult to separate AgNPs from these added reagents thoroughly, which greatly limits the application of produced AgNPs.[12]

Lignin is a complex phenolic polymer occurring in higher plant tissues, and it is the second most abundant natural polymer after cellulose. It is a three-dimensional amorphous polymer consisting of methoxylated phenyl-propane substructures.[13] As the waste in pulp and paper industry, it is often used as fuel for the energy balance of the pulping process,[14] and extensive research was devoted to the development of lignin-

**Received:** June 30, 2014
**Accepted:** August 21, 2014
**Published:** August 21, 2014

  

containing polymeric materials. So far, lignin was utilized in the application of cement and building engineering, water treatment, adhesive, agriculture, food, and medicine.[15−20] It is worth noting that lignin has many functional groups, such as hydroxyl, carbonyl, and aldehyde groups,[21] which can be used for the reducing formation of nano metal, and the spatial three-dimensional structure is able to stabilize the nano metal. But to our knowledge, there is no report about preparing AgNPs by using lignin as environment-friendly reducing and stabilizing agents.

Here, lignin was used as green reducing and stabilizing agents to prepare stable AgNPs under microwave irradiation, which provided uniform heating around the nanoparticles and assisted the digestive ripening of such particles without aggregation.[22] This method was conducted without other chemical reducing agents or stabilizing agents, such as sodium borohydride and hydrazine hydrate. More importantly, it took high-value utilization of lignin, the agricultural and forestry residues, to prepare AgNPs. The effects of the reaction conditions on the synthesis of AgNPs were investigated. The redispersibility of AgNPs both in water and in ethanol was observed after centrifugation for the removal of lignin. The structural change of lignin during the reaction was characterized, and then the mechanism was conjectured. Finally, the selective and sensitive detection toward $Hg^{2+}$ was measured with other metal ions ($Na^+$, $K^+$, $Ca^{2+}$, $Al^{3+}$, $Fe^{3+}$, $Co^{2+}$, $Ni^{2+}$, $Li^+$, $Cr^{3+}$, $Ag^+$, $Au^{3+}$, $Fe^{2+}$, $Mg^{2+}$, $Cu^{2+}$, $Zn^{2+}$, $Mn^{2+}$, $Ba^{2+}$, $Pb^{2+}$, and $Cd^{2+}$) as contrast.

## 2. EXPERIMENTAL SECTION

**2.1. Materials and Equipment.** Acetic acid lignin was obtained through the method of acetic acid pulping.[23] Ammonia solution (25%) was purchased from Guanghua Sci-Tech Co., Ltd. (Guangdong, China). Silver nitrate was supplied by the Institute of Fine Chemicals (Shanghai, China). An XH-100B microwave synthesis system was purchased from the Beijing Xianghu Sci-Tech Co., Ltd. (Beijing, China). All other chemical reagents were analytical reagents.

**2.2. Purification of Acetic Acid Lignin.** First, 70 g of acetic acid lignin was mixed uniformly into a beaker with 500 mL of glacial acetic acid. The mixture was filtered, and the filtrate was collected. Then, the filtrate was slowly poured into a beaker with 4 L of ultrapure water with mechanical stirring until the lignin was uniformly dispersed. Afterward, the mixture was filtered after standing for 12 h, and the residue was washed with 60−70 °C water until the pH of the filtrate was 7. The residue was collected and dried by lyophilization. Finally, the refined lignin was obtained.

The refined lignin powders (5 mg) were hydrolyzed with 1.475 mL of 6% sulfuric acid at 105 °C for 2.5 h. Then the sugar analysis of lignin was conducted by high-performance anion exchange chromatography (HPAEC; Dionex ICS-3000, Thermo Fisher Scientific, Inc., Waltham, MA). The sugars were separated in 18 mM NaOH (carbonate free and purged with nitrogen) with postcolumn addition of 0.3 M NaOH at a rate of 0.5 mL/min. Calibration was performed with a standard solution of L-rhamnose, L-arabinose, D-glucose, D-xylose, D-mannose, D-galactose, glucuronic acid, and galacturonic acid. The refined lignin was made up of 2.85% xylose, 0.90% arabinose, 0.62% glucose, and 0.25% galactose. So, the purity of lignin was near to 95.59%.

**2.3. Preparation of AgNPs.** First, a few drops of diluted sodium hydroxide were added to aqueous silver nitrate (1 mmol/mL) to precipitate $Ag^+$ to give silver oxide, $Ag_2O$, completely. Then, aqueous ammonia (25 wt %) was added until all of the brown silver oxide was dissolved. At this point, the $Ag^+$ existed as $[Ag(NH_3)_2]OH$ in the clear mixture.

Next, 0.3 g of refined lignin was dissolved in 1% NaOH solution (1 mg/mL). Then, 25 mL of $[Ag(NH_3)_2]OH$ solution was added into the above solution and reacted under microwave irradiation with the designed time and temperature. After the reaction, the colloidal AgNPs were dialyzed until there was no $Ag^+$, and then AgNPs were obtained after lyophilization at −40 °C. During the reaction, a series of AgNPs were obtained by controlling the different ratios of lignin to $Ag^+$, reaction temperatures, and heating time. The obtained composites were designated as LAg1−LAg12, as shown in Table 1.

**Table 1. Samples with Different Reaction Conditions**

| samples | $T$ (°C) | lignin/$Ag^+$ (50 mg/mM) | $t$ (min) |
|---|---|---|---|
| LAg1 | 80 | 0.2 | 10 |
| LAg2 | 80 | 0.25 | 10 |
| LAg3 | 80 | 0.3 | 10 |
| LAg4 | 80 | 0.35 | 10 |
| LAg5 | 80 | 0.4 | 10 |
| LAg6 | 50 | 0.3 | 10 |
| LAg7 | 60 | 0.3 | 10 |
| LAg8 | 70 | 0.3 | 10 |
| LAg9 | 60 | 0.3 | 5 |
| LAg10 | 60 | 0.3 | 15 |
| LAg11 | 60 | 0.3 | 20 |
| LAg12 | 60 | 0.3 | 30 |

**2.4. Selective and Sensitive Detection of $Hg^{2+}$.** The well-dispersed lignin−AgNP complex solution with a concentration of 0.02 mg/mL was prepared, and different volumes (0, 50, 100, 150, 200, 250, 300, 350, 400, 450, and 500 μL) of $Hg^{2+}$ ($HgCl_2$, $10^{-3}$ mol/L) were added into 3 mL of lignin−AgNP solution. By contrast, 500 μL of many kinds of metal ions solutions (NaCl, KCl, $CaCl_2$, $Al(NO_3)_3\cdot 9H_2O$, $FeCl_3\cdot 6H_2O$, $Co(NO_3)_2\cdot 6H_2O$, $Ni(NO_3)_2\cdot 6H_2O$, LiCl, $Cr(NO_3)_3\cdot 9H_2O$, $AgNO_3$, $HAuCl_4$, $FeSO_4\cdot 7H_2O$, $MgCl_2\cdot 6H_2O$, $CuSO_4\cdot 5H_2O$, $Cd(NO_3)_2\cdot 4H_2O$, $ZnSO_4\cdot 7H_2O$, $MnCl_2\cdot 4H_2O$, $BaCl_2\cdot 2H_2O$, $HgCl_2$, $Pb(NO_3)_2$ and $Cd(NO_3)_2\cdot 4H_2O$; $10^{-3}$ mol/L) was added into 3 mL of lignin−AgNP solution under the same conditions, respectively, and 3 mL of AgNPs solution mixed with 500 μL of $H_2O$ served as a blank. To ensure that there was no interference by other metal ions, 250 μL of other metal ions ($10^{-3}$ mol/L) were added to 3 mL of AgNPs solutions mixed with 250 μL of $Hg^{2+}$, respectively, and 3 mL of AgNP solution mixed with 250 μL of $Hg^{2+}$ and 250 μL of $H_2O$ served as a blank. Within seconds after adding metal ions, we measured the mixtures using a UV−vis spectrophotometer (TU-1810, Beijing, China).

**2.5. Characterization of AgNPs and Lignin.** UV−vis spectra of AgNPs were collected on a spectrophotometer. The spectral scanning range was 600−300 nm, the speed was fast, and the scan interval was 0.5 nm. The particle size distributions of AgNPs were obtained by a Malvern laser particle size analyzer (3000 HSA, Malvern, England). Ultrasonic treatment was required before measuring. The shape and distribution of the AgNPs were observed by transmission electron microscopy (TEM; Jem-2100, Japan), which worked with an accelerating voltage of 200 kV. A few drops of the suspended AgNPs were placed on a copper grid coated with ultrathin carbon film. The crystal structure of AgNPs was investigated by a D8 ADVANCE X-ray diffractometer (Bruker, Germany), in which the nickel-filtered Cu K$\alpha$ radiation ($\lambda$ = 0.15406 nm) was generated at 40 kV and 40 mA. Samples were scanned at a step size of 0.0195° in the range 5−90° (2$\theta$). The X-ray photoelectrons spectroscopy (XPS) spectra of the samples were obtained by an AXIS Ultra DLD spectrometer (Kratso, England) using Mg K$\alpha$ radiation (h$\gamma$ = 1253.6 eV) with a step size of 0.1 eV.

FT-IR spectra were measured by a Tensor 27 (Bruker, Germany) under dry air at room temperature by a KBr pellet method. Each sample was scanned from 4000 to 400 $cm^{-1}$ with a resolution of 4 $cm^{-1}$. $^1H$ NMR and $^{13}C$ NMR spectra were recorded on a Bruker-Spectrospin 300 UltraShield spectrometer (Bruker, Germany), and the solvent was NaOD. The results of GC-MS were recorded by an HP6890GC/5973MS analyzer (Agilent, USA) with a quartz capillary column (30 m × 0.25 mm × 0.25 μm). The temperature of column

was increased as follows: (a) 90 °C for 10 min; (b) from 90 to 205 °C at a rate of 5 °C/min; (c) from 205 to 280 °C at a rate of 8 °C/min; and (d) 280 °C for 15 min. Helium was used as carrier gas with a split ratio of 5:1. The dialysate of products was acetylated before measuring.

## 3. RESULTS AND DISCUSSION

**3.1. Effects of the Synthesis Conditions on the Formation of AgNPs.** *3.1.1. Different Ratios of Lignin to $Ag^+$.* UV−vis spectroscopy is one of the most important techniques to investigate the formation of metal nanoparticles.[24] As illustrated in the UV−vis spectra in Figure 1a,

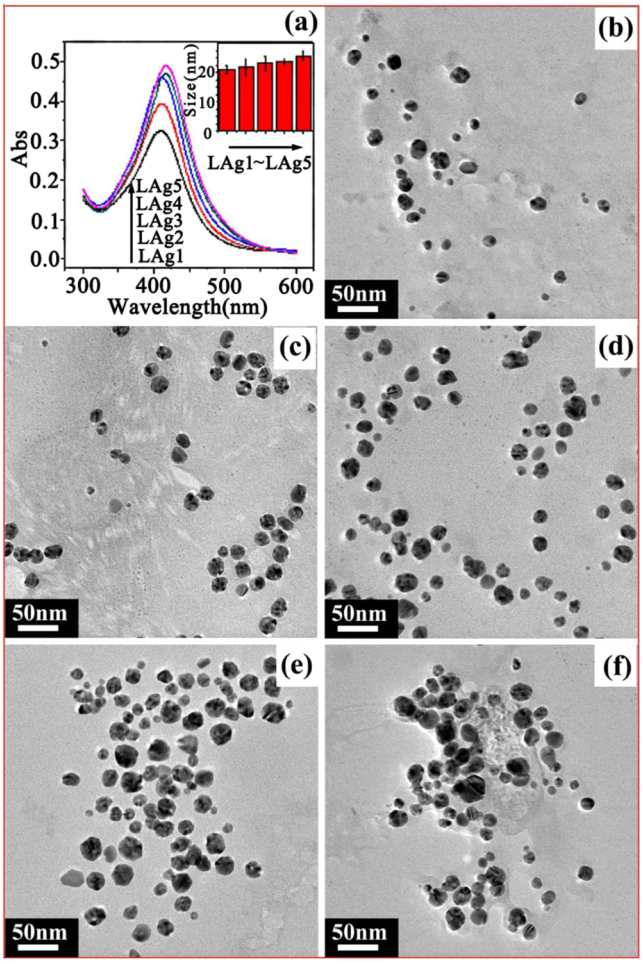


**Figure 1.** Results with different ratios: (a) UV−vis and (inset) Malvern particle size histograms; (b−f) TEM images of LAg 1−LAg 5, respectively.

a strong surface plasmon resonance was centered at approximately 416 nm, revealing the formation of AgNPs.[25] The sharp plasmon peak (with a full width at half-maximum of 70−80 nm) indicated a very narrow distribution in particle sizes.[26] Furthermore, the shape of the plasmon band was symmetrical, suggesting that the AgNPs are spherical and monodisperse.[27] Figure 1a shows that the absorbance of the spectrum increased with the increasing amount of $Ag^+$, indicating that the amount of AgNPs increased with the increasing amount of $Ag^+$. It was clear that the red shift of the peak appeared when the ratio of lignin to $Ag^+$ increased to 50 mg/0.35 mM, indicating that the average size of AgNPs was enlarged or AgNPs aggregated,[28] presumably due to the higher probability of particle collisions.[29] Meanwhile, the AgNPs have started to precipitate during the reaction, observing from the flask, when the ratio of lignin to $Ag^+$ arrived to 50 mg/0.35 mM. The results of Malvern particle size histograms showed that the average sizes of AgNPs increased slightly with the increasing amount of $Ag^+$, which was the same as the result of UV−vis analysis. Figure 1b−f shows the TEM images of AgNPs, in which AgNPs appeared almost spherical. The average particle sizes and the amount of AgNPs increased slightly with the increasing amount of $Ag^+$. The particles started to aggregate and even precipitated when the ratio of lignin to $Ag^+$ was up to 50 mg/0.35 mM, and the increase in the concentration of AgNPs promoted their aggregation. Therefore, the ratio of lignin to $Ag^+$ of 50 mg/0.3 mM was considered as the optimum ratio condition, which was in agreement with the first two analyses.

*3.1.2. Different Reaction Temperatures.* Figure 2a shows the spectra at different reaction temperatures. It was obvious

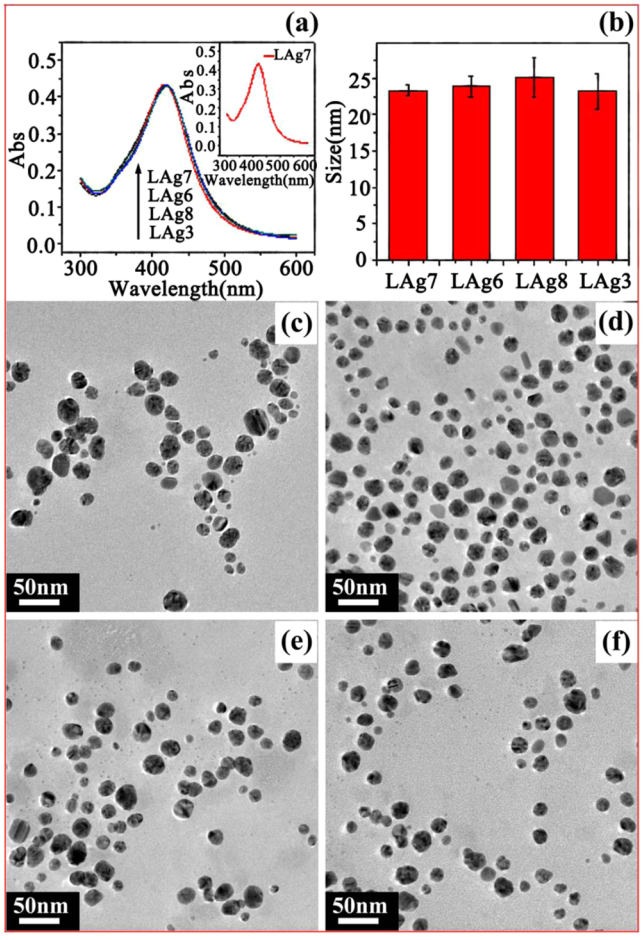


**Figure 2.** Results with different temperatures: (a) UV−vis; (b) Malvern particle size histograms; (c−f) TEM images of LAg 6−LAg 8 and LAg 3, respectively.

that the spectra were similar, among which, LAg7 was the smoothest spectrum, and it meant that the amount of AgNPs was hardly related to the reaction temperatures. It was noted that the particles dispersed most uniformly in 60 °C. Figure 2b illustrates the particle size histograms of AgNPs prepared at different temperatures. It was easy to see that the average particle sizes of AgNPs were similar, 23−25 nm, indicating that the formation of AgNPs was not affected by temperature, which


dx.doi.org/10.1021/am504188k | ACS Appl. Mater. Interfaces 2014, 6, 16147−16155

corresponded to the UV−vis analysis. Figure 2c−f shows the TEM images of AgNPs prepared at different reaction temperatures. The AgNPs grew well without aggregation below 80 °C. The reaction of AgNPs can be completed within minutes under microwave irradiation,[30] so it was not surprising that the particle sizes were nearly similar and the particles were almost spherical, further demonstrating that the reaction temperature had little influence on the shape and size of AgNPs. The particles dispersed most uniformly at 60 °C. Thus, 60 °C was considered the optimum reaction temperature, combining the results of UV−vis analysis.

*3.1.3. Different Heating Time.* As shown in the UV−vis spectra of Figure 3a, heating time had little affect on the plasmon intensity, the reaction was at a fast speed, and it ran to the top in 10 min. The same full width at half-maximum illustrated that the amount and distribution of particles were similar. The Malvern particle size histogram (Figure 3a, inset) shows the particle sizes of AgNPs at different heating times. The average particle size of AgNPs ranged from 23 to 25 nm for different heating time, which meant that the process of preparing AgNPs was at a fast speed, and the heating time had little influence on the preparation of AgNPs, which agreed completely with the results of UV−vis analysis. The TEM images of AgNPs of different heating times are shown in Figure 3b−f, revealing that the particle sizes were similar to each other, though the heating time was different This may be due to the particles' fast growth rate; the particles reached their size limit within minutes. The particles did not aggregate in the first 20 min, and they dispersed mostly uniformly in 10 min. However, when the heating time was up to 30 min, the particles began to aggregate obviously. Because AgNPs were embedded in the three-dimensional spatial structure of lignin (Figure 4a), and embedding continued to increase with the increasing time of microwave exposure,[31] the particles began to aggregate as they reached their embedding limit. Therefore, the optimum heating time was 10 min, combining the UV−vis and particle size analyses.

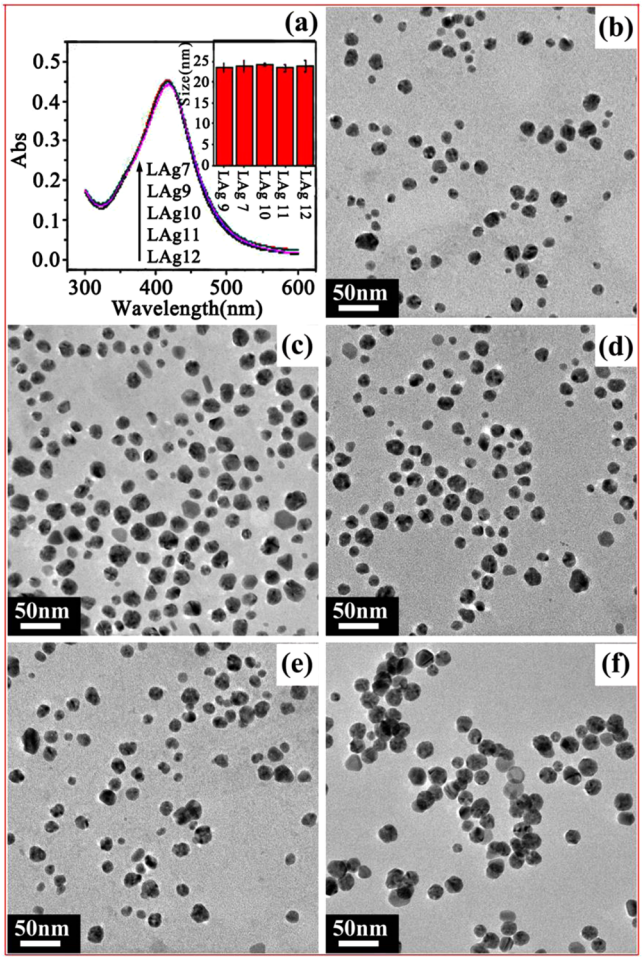


**Figure 3.** Results with different heating times: (a) UV−vis and (inset) Malvern particle size histograms; (b−f) TEM images of LAg 9, LAg 7, and LAg 10−LAg 12, respectively.

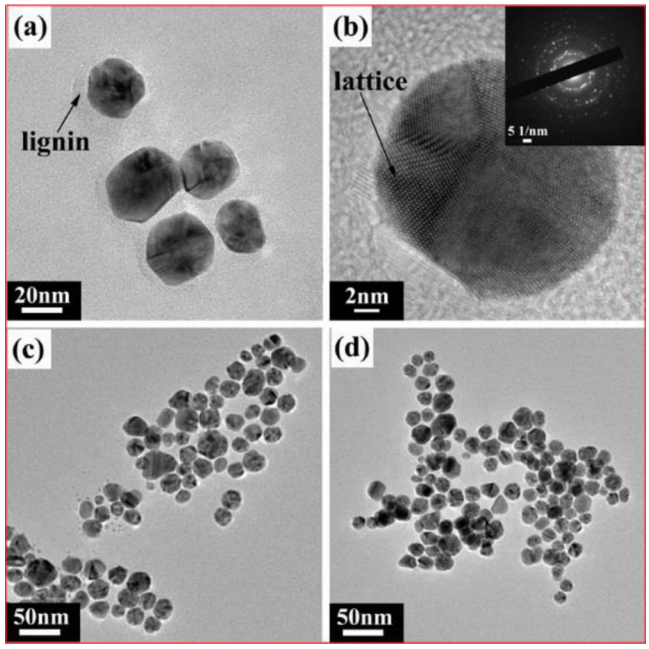


**Figure 4.** TEM images of AgNPs (a) capped by lignin, (b) in high resolution, (b, inset) selected area electron diffraction of AgNPs, (c) dissolved into water after centrifugation, and (d) dissolved into ethanol after centrifugation.

*3.1.4. Optimum Conditions.* Based on the above analyses of UV−vis, Malvern particle sizes, and TEM, when lignin acted as reducing and stabilizing agent, AgNPs with a diameter of around 24 nm were obtained rapidly within minutes under microwave irradiation. The amount of AgNPs increased with the increasing amount of $Ag^+$, but the shape and size changed little. Moreover, temperature and heating time had little influence on the shape and size of AgNPs, which were almost spherical. In addition, the optimum conditions for synthesizing AgNPs was a ratio of 50 mg of lignin to 0.3 mM of $Ag^+$, a reaction temperature of 60 °C, and a heating time of 10 min.

**3.2. Structure and Morphology of Lignin−AgNP Complex.** Figure 4a shows that AgNPs were capped by lignin. Lignin is a three-dimensional spatial polymer, which can provide good space for the growth of AgNPs by wrapping. Lignin can also stabilize AgNPs and prevent aggregation of AgNPs. Figure 4b shows the regular lattice of AgNPs, demonstrating that AgNPs existed in the crystalline state. The inset of Figure 4b selected area electron diffraction of AgNPs illustrated that AgNPs came in single-crystal structures. Each circle was overlapped by several hexagonal lattices.

Figure 4c,d shows the TEM images of AgNPs dispersed into water and ethanol after being centrifuged to remove lignin, respectively. The particles were able to disperse well both in water and ethanol again after centrifugation, which is significant for the reuse of AgNPs and the recycling of precious metal.

The XRD patterns of the lignin−AgNP complex are shown in Figure 5a. There were five peaks at $2\theta$ = 38.11°, 44.32°, 64.42°, 77.49°, and 81.58° in the patterns, and these peaks were the same as JCPDS (No. 89−3722), which corresponded to the (111), (200), (220), (311), and (222) lattice planes of Ag.[32] This further indicated that AgNPs existing in the crystalline state could be obtained via our environmental-friendly method. In addition, by comparing the intensity of peaks, the amount of AgNPs increased with the increasing amount of $Ag^+$, which was in agreement with the foregoing results.

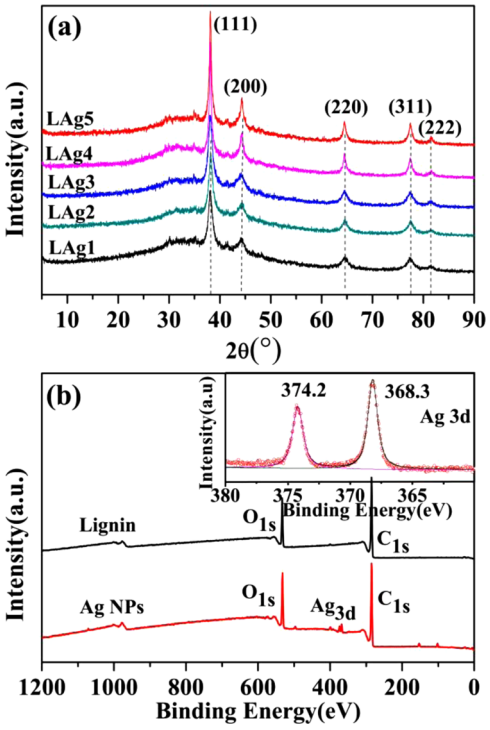


**Figure 5.** (a) XRD patterns of the lignin−AgNP complex and (b) XPS spectra of original lignin and the lignin−AgNP complex.

Figure 5b depicts the XPS spectra of original lignin and the lignin−AgNPs complex. The lignin−AgNP complex was dialyzed to remove $Ag^+$ without reacting before measurement. Besides O and C elements in lignin, the spectrum of the lignin−AgNP complex also contained elemental Ag, which indicated that AgNPs were prepared successfully. Binding energies were calibrated by using the containment carbon (C1s = 284.6 eV). The high-resolution XPS spectrum of Ag 3d electron binding energy could only be divided into two peaks. And the two peaks occurring at 374.2 and 368.3 eV corresponded to Ag $3d_{5/2}$ and $3d_{3/2}$ binding energies, respectively.[33] The results further indicated that the AgNPs existed in the crystalline state,[34−36] as shown in Figure 4b.

**3.3. Structure Characterization of Lignin before and after Reaction.** To illustrate the structural change of lignin during the reaction, Figure 6 shows the FT-IR spectra of lignin and the products with and without dialysis after removing AgNPs by centrifugation. The peak at 3426 $cm^{-1}$ was the characteristic absorption of O−H stretching, and compared to that of original lignin, the peak in the spectrum of products without dialysis (Figure 6a) became stronger, but the peak of products with dialysis changed little, indicating that a part of lignin transformed to alcohol in the process of reaction and was permeated out by dialysis. The peaks at 3005−2843 $cm^{-1}$ were the absorption of $-CH_2-$ and $-CH_3$ stretching, but the intensity in Figure 6a,b became lower, indicating that $-CH_2-$ and $-CH_3$ belonging to the chain of lignin can be cut off and permeated out by dialysis. The peak at 1732 $cm^{-1}$ in Figure 6c, belonging to the absorption of nonconjugated C═O stretching of ester, disappeared after reaction, and a new peak belonging to the absorption of C═O stretching of carboxyl occurred at 1645 $cm^{-1}$ in Figure 6a, which was most likely due to the nonconjugated C═O of ester in lignin was transformed to carboxyl during the reaction. The peaks at 1603, 1512, and 1421 $cm^{-1}$ belonged to the absorption of benzene ring stretching, and the peak at 1459 $cm^{-1}$ belonged to the unsymmetrical bending vibration of C−H in methoxyl,[37] while after reaction, they were all covered up by the strong absorption of C−H stretching of alkane or alkene at 1448 and 1384 $cm^{-1}$ in Figure 6a, which indicated that in the process of preparing AgNPs, the side chains of lignin were broken and changed to some micromolecular materials, such as hydrocarbon, and they were permeated out by dialysis. The intensity of the peak at 1234 $cm^{-1}$ belonging to the absorption of C−H stretching of Syringyl (*S*) ring became lower after reaction (Figure 6b), showing that some *S* units of lignin changed to other kinds of benzene ring or dropped out. But the peak was not shown in Figure 6a because it was covered up by the strong absorption of the C−H stretching of alkane or alkene.

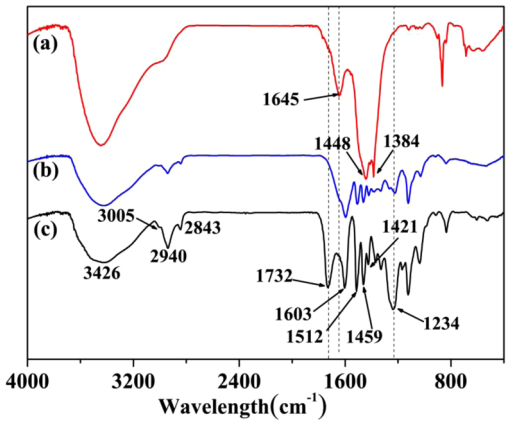


**Figure 6.** FT-IR spectra of (a) products without dialysis, (b) products with dialysis, and (c) original lignin.

We further studied of the structural change of lignin with $^1H$ NMR and $^{13}C$ NMR, and the products with and without dialysis after removing AgNPs by centrifugation are shown in Figure 7. Figure 7a−c shows the $^1H$ NMR spectra of lignin and the products. The lignin was connected by $\beta$−O−4, $\beta$−5, $\beta$−$\beta$, and $\beta$−1, mainly by the analysis of signals.[38−40] As we compared curve b to curve c (Figure 7), it was obvious that the signals at 8.0−6.0 ppm and 2.0−0.36 ppm weakened relatively or even disappeared because of the destruction of lignin during the reaction. The signal of 7.96 ppm may be caused by the H in the single benzene ring dropping out due to the shedding of the benzene ring during the reaction. The new signals at 6.89−6.73 ppm in Figure 7a belonged to the H in the benzene ring with $C_4-O-R$ (R is alkyl), revealing that the H of −OH in $C_4$ of the


dx.doi.org/10.1021/am504188k | ACS Appl. Mater. Interfaces 2014, 6, 16147−16155

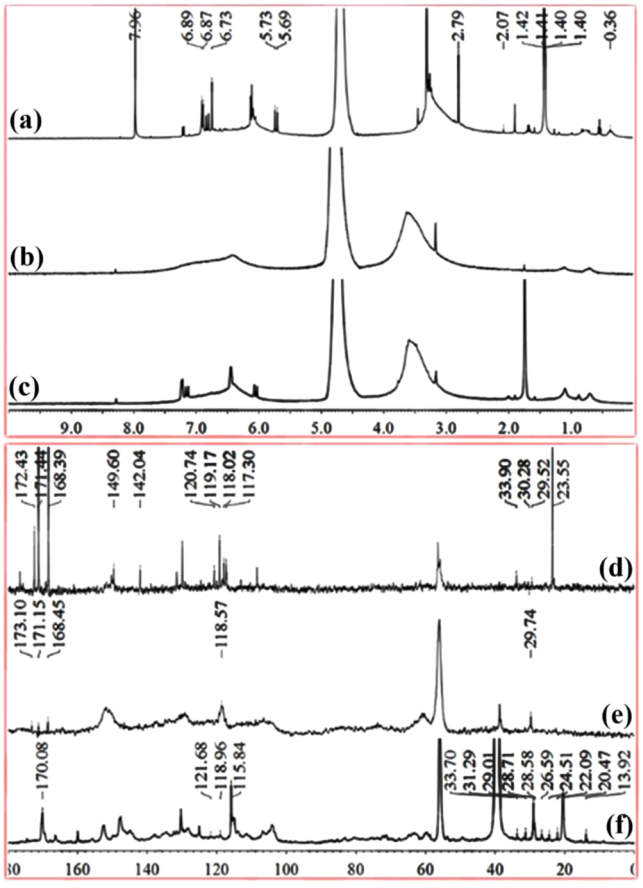


**Figure 7.** $^{1}$H NMR spectra of (a) sample without dialysis, (b) sample with dialysis, and (c) original lignin. $^{13}$C NMR spectra of (d) sample without dialysis, (e) sample with dialysis, and (f) original lignin.

benzene ring was replaced by other groups, and the side chain connected this benzene ring was disrupted. The signals at 5.73−5.69 ppm and the signal at 2.79 ppm, which only occurred in the $^{1}$H NMR spectra of the sample without dialysis (Figure 7a), belonged to the H in the carbon chain and in $-OCH_3$, respectively, illustrating that the side chains of lignin were disrupted and transformed to small units with $-OCH_3$, which is in agreement with the results of FT-IR analysis. In the spectra of 2.07−0.36 ppm belonging to the H in the fatty substance, some new signals came in while some of the intrinsic signals disappeared (Figure 7b), which illustrated that some of side chains were broken into fatty substance during the process of preparing AgNPs. Figure 7d−f reveals the $^{13}$C NMR spectra of lignin. In the range of 168.39−173.10 ppm, only one signal of 170.08 ppm occurred in original lignin, while the products came in several signals, and the signals in this range belonged to C═O in aliphatic chain, indicating that lignin was oxidized during the reaction. The signals at 149.60 and 142.04 ppm were C in etherified and nonetherified benzene ring, respectively. Among these signals, the signal at 142.04 ppm only occurred in the $^{13}$C NMR spectrum of lignin without dialysis (Figure 7d), revealing that the side chains of lignin were broken and the separate small units with benzene ring disappeared through dialysis. The signals at 120.74−117.30 ppm in Figure 7d and the only signal at 118.57 ppm in Figure 7e belonged to the C in the Guaiacyl (*G*) unit, showing that partial *G* units changed to other kinds of benzene or dropped out. In Figure 7f, the signals at 40−20 ppm were $-CH_3$ and $-CH_2-$ in an aliphatic chain, while Figure 7d,e shows fewer signals in these areas, illustrating that the structure of side chains of lignin were disrupted during the reaction, which was in agreement with the analysis of FT-IR and $^{1}$H NMR.

Because the difference in the results of FT-IR, $^{1}$H NMR, and $^{13}$C NMR occurred between the products with dialysis and the products without dialysis, it can be deduced that micromolecular materials were produced during the reaction. To further explore the mechanism of the AgNPs formation, we investigated the composition of the dialysate of the products by analytical GC-MS; the chromatogram and results are shown in Figure 8. Signals 1, 4, 7, and 8 demonstrated that the side

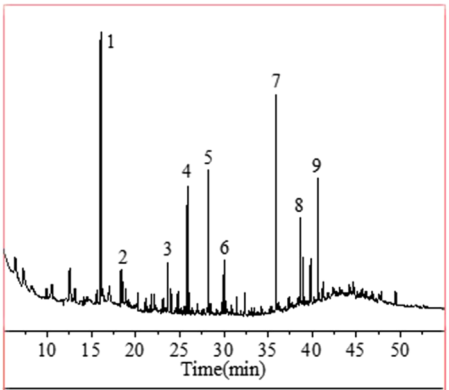


| NO. | Retention time (min) | Compound |
|---|---|---|
| 1 | 16.046 | Hexanoic acid |
| 2 | 18.339 | Triacetin |
| 3 | 23.601 | 4-Acetoxy-3-methoxybenzaldehyde |
| 4 | 25.857 | Dodecan-1-yl acetate |
| 5 | 28.225 | 4-Acetoxy-3,5-dimethoxybenzaldehyd |
| 6 | 30.013 | 1-(4-Hydroxy-3,5-dimethoxyphenyl)-ethanone |
| 7 | 35.909 | Palmitoyl chloride |
| 8 | 38.616 | 1-Hexadecene |
| 9 | 40.640 | 2,2'-Methylenebis(4-methyl-6-tert-butylphenol) |

**Figure 8.** GC-MS results of dialysate of products.

chains of lignin were disrupted, while signals 3, 5, 6, and 9 illustrated that the side chains of the benzene rings were disrupted and the separating benzene rings were permeated out during dialysis. Signal 3 represented the break of *G* units, and signals 5 and 6 represented the break of *S* units. The results demonstrated that the structure of lignin was partly broken during the process of preparing AgNPs, which was in agreement with the FT-IR and NMR results.

**3.4. Suggested Reaction Mechanism of Lignin to Synthesize AgNPs.** According to the analysis of FT-IR, $^{1}$H NMR, $^{13}$C NMR, and GC-MS, lignin acting as a reducing agent for the preparation of AgNPs might be because the phenolic lignin of $\alpha$-aryl ether and alkyl ether changed in alkaline conditions under microwave irradiation as follows: First, the

**Scheme 1. Process of Preparing AgNPs with Lignin as Reducing and Stabilizing Agent**

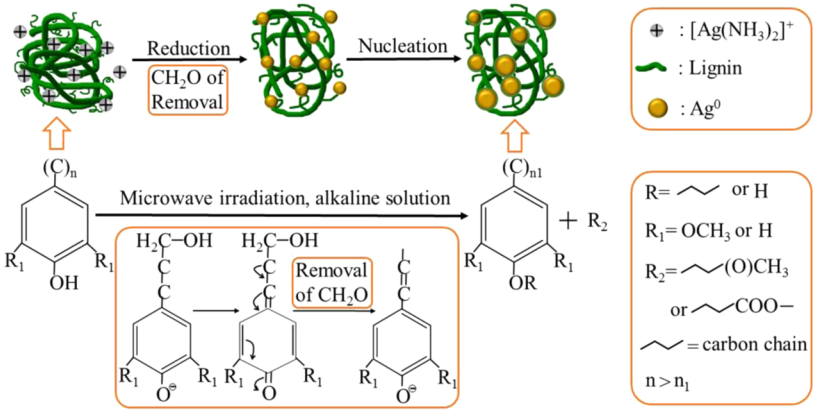


phenolic structure generated anions, which promoted the fracture of the ether bond, and quinone methide was formed. Second, the inductive effect was caused by the electron-acceptor of carbonyl in quinone methide, leading to reducing the density of the electron cloud around $\beta$−C and the linkage between $\beta$−C and $\gamma$−C of primary alcohol. Finally, formaldehyde, which was able to reduce $Ag^+$ to $Ag^0$, dropped out. The course is shown in Scheme 1.

**3.5. Selective and Sensitive Detection for $Hg^{2+}$.** The sensitive detection for $Hg^{2+}$ was investigated with different volumes of $Hg^{2+}$ ($10^{-3}$ mol/L), as shown in Figure 9a. As the $Hg^{2+}$ volume increased, the maximum absorbance of the spectrum decreased, and a blue shift of the peaks appeared. When the volume was up to 500 $\mu$L, equating to the concentration of 500 nM, there was no peak in the spectrum. The results demonstrate that $Hg^{2+}$ was sensitive to AgNPs.

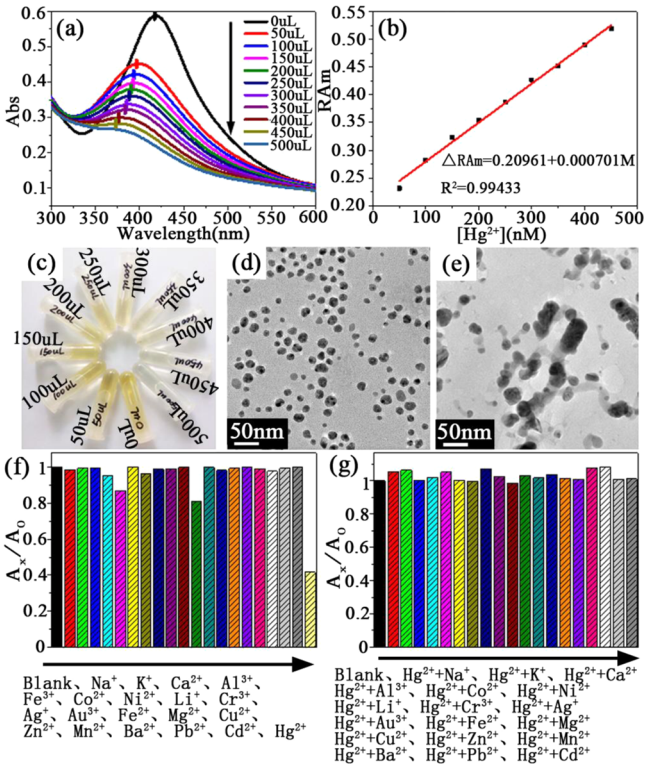


**Figure 9.** (a) UV−vis spectra of AgNPs after adding different volumes of $Hg^{2+}$ ($Hg^{2+}$ concentration: $10^{-3}$ mol/L); (b) the linear relationship between the absorbance and $Hg^{2+}$ concentration; (c) photos of AgNPs solution after adding different volumes of $Hg^{2+}$; (d and e) TEM images of AgNPs before and after adding $Hg^{2+}$, respectively; (f) $A_x/A_0$ values of AgNPs mixed with different metal ions; and (g) $A_x/A_0$ values of AgNPs mixed with $Hg^{2+}$ and other metal ions.

The linear relationship between the absorbance and $Hg^{2+}$ concentration over the range of 50−450 nM is shown in Figure 9b, and it followed the regularity by the linear regress equation: $RA_m = 0.20961 + 0.00701M$, $R^2 = 0.99433$. $RA_m$ was defined as $\{[A_{max}\ (0) - A_{max}\ (M)]/A_{max}\ (0)\}$, where $A_{max}$ (M) was the maximum absorbance of the spectrum at molar concentration M of $Hg^{2+}$. The limit of detection (LOD) was calculated to be 23 nM (S/N = 3).

Figure 9c shows the photos of AgNPs with different volumes of $Hg^{2+}$, corresponding to Figure 9a, within seconds. The color of the solution decreased gradually from yellow to colorless with an increasing amount of $Hg^{2+}$. When 500 $\mu$L of $Hg^{2+}$ ($10^{-3}$ mol/L) was added, the color of solution was colorless. So, $Hg^{2+}$ can be rapidly detected with lignin−AgNPs by monitoring the color change with naked eye.

Figure 9d,e shows the TEM images of AgNPs, which were prepared more than a month before and after adding $Hg^{2+}$, respectively. It was found that lignin−AgNPs still dispersed well (Figure 9d), and so, the obtained lignin−AgNPs were stable. In Figure 9e, the aggregated and typical tadpole-shaped particles were obtained, probably because the van der Waals interaction between lignin and AgNPs was weaker than the complexation between the carboxyl/hydroxyl groups of lignin and $Hg^{2+}$. Then, capping of the AgNPs by lignin was eliminated, and the AgNPs were bare, resulting in their aggregation.[41] At the same time, some $Hg^{2+}$ may have deposited or grown selectively on the lattice planes of the AgNPs, forming the tadpole-shaped particles.[42−44] The mechanism is shown in Scheme 2.

The selective detection for $Hg^{2+}$ was investigated with different metal ions (Figure 9f,g). In Figure 9f, $A_0$ was the absorbance of blank (AgNPs mixed with 500 $\mu$L $H_2O$) at 419 nm, and $A_x$ was the absorbance of AgNPs mixed with 500 $\mu$L metal ion x. The histogram of AgNPs solution mixed with $Hg^{2+}$ was much lower than others due to the higher affinity between carboxyl/hydroxyl groups of lignin and $Hg^{2+}$ than other metal ions,[41,45,46] illustrating that other metal ions except for $Hg^{2+}$ had little influence on AgNPs. The AgNPs solutions mixed with $Hg^{2+}$, and other metal ions were also measured in Figure 9g, where $A_0$ meant the absorbance of blank (AgNPs mixed with 250 $\mu$L $Hg^{2+}$ and 250 $\mu$L $H_2O$) at 383 nm, and $A_x$ was the absorbance of AgNPs mixed with 250 $\mu$L $Hg^{2+}$ and 250 $\mu$L


dx.doi.org/10.1021/am504188k | ACS Appl. Mater. Interfaces 2014, 6, 16147−16155

**Scheme 2. Detection Mechanism of Lignin−AgNP Complex for $Hg^{2+}$**

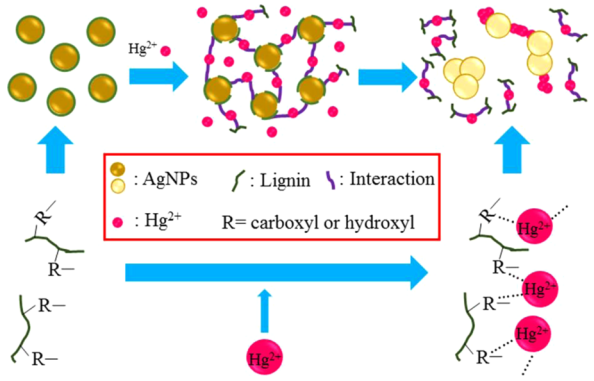


other metal ion x. The absorbance ratio after adding other metal ions were close to the absorbance ratio of blank, indicating that other metal ions had little effect on the detection of $Hg^{2+}$. The results confirm that the prepared AgNPs had the selective detection capacity for $Hg^{2+}$.

## 4. CONCLUSIONS

In this study, we prepared AgNPs in lignin alkaline aqueous solutions by microwave irradiation using Tollens' reagent as the silver source without adding additional reducing and stabilizing agents. The amount of AgNPs increased with the increasing amount of $Ag^{+}$, but there was not much difference between the different reaction temperatures and heating times. The shape and size of AgNPs were hardly affected by the different conditions used during the reaction, such as the amount of $Ag^{+}$, reaction temperature, and heating time. AgNPs still dispersed well both in water and in ethanol, even after centrifugation, which contributed to the further research of cyclic utilization for noble metals. During the reaction, the side chains of lignin were disrupted into small molecules, such as hydrocarbon and alcohol, and some of the benzene rings dropped out. Moreover, etherification existed in $C_4$ of the benzene ring, and oxidization made the C structure in lignin transform to carboxyl. The resultant lignin−AgNPs had highly sensitive and selective detection toward $Hg^{2+}$ with a LOD concentration of 23 nM, but they had little effect on other metal ions. The color of lignin−AgNPs changed from yellow to colorless with increasing amount of $Hg^{2+}$, which made it very easy and quick to detect $Hg^{2+}$ in the living environment. Therefore, the study provided not only a direction for the valuable utilization of a biomass resource but also a novel method for synthesis of noble metal nanoparticles, which can be used to detect $Hg^{2+}$ sensitively and selectively in our living environment.

## AUTHOR INFORMATION

### Corresponding Author

*E-mail: xyw@scut.edu.cn. Tel.: +86-136-2284-0981.

### Notes

The authors declare no competing financial interest.

## ACKNOWLEDGMENTS

This work was financially supported by the Program for New Century Excellent Talents in University (NCET-13-0216), the Science and Technology Project of Guangzhou City in China (No. 2012J2200018), the Fundamental Research Funds for the Central Universities, SCUT (No. 2014ZG0011), and the State Key Laboratory for Modification of Chemical Fibers and Polymer Materials, Dong Hua University (No. LK1223).

## REFERENCES

(1) Lee, J. S.; Han, M. S.; Mirkin, C. A. Colorimetric Detection of Mercuric Ion ($Hg^{2+}$) in Aqueous Media Using DNA-Functionalized Gold Nanoparticles. *Angew. Chem.* **2007**, *119*, 4171−4174.

(2) Kim, T. H.; Lee, J.; Hong, S. Highly Selective Environmental Nanosensors Based on Anomalous Response of Carbon Nanotube Conductance to Mercury Ions. *J. Phys. Chem. C* **2009**, *113*, 19393−19396.

(3) Sun, Z. Z.; Zhang, N.; Si, Y. M.; Li, S.; Wen, J. W.; Zhu, X. B.; Wang, H. High-Throughput Colorimetric Assays for Mercury(II) in Blood and Wastewater Based on the Mercury-Stimulated Catalytic Activity of Small Silver Nanoparticles in a Temperature-Switchable Gelatin Matrix. *Chem. Commun. (Cambridge, U.K.)* **2014**, *50*, 9196−9199.

(4) Duan, J. L.; Yin, H. Z.; Wei, R. R.; Wang, W. W. Facile Colorimetric Detection of $Hg^{2+}$ Based on Anti-Aggregation of Silver Nanoparticles. *Biosens. Bioelectron.* **2014**, *57*, 139−142.

(5) Rastogi, L.; Sashidhar, R. B.; Karunasagar, D.; Arunachalam, J. Gum Kondagogu Reduced/Stabilized Silver Nanoparticles as Direct Colorimetric Sensor for the Sensitive Detection of $Hg^{2+}$ in Aqueous System. *Talanta* **2014**, *118*, 111−117.

(6) Jain, P. K.; Huang, X. H.; EI-Sayed, I. H.; EI-Sayed, M. A. Review of Some Interesting Surface Plasmon Resonance-Enhanced Properties of Noble Metal Nanoparticles and Their Applications to Biosystems. *Plasmonics* **2007**, *2*, 107−118.

(7) Sharma, V. K.; Yngard, R. A.; Lin, Y. Silver Nanoparticles: Green Synthesis and Their Antimicrobial Activities. *Adv. Colloid Interface Sci.* **2009**, *145*, 83−96.

(8) Liu, F. K.; Hsu, Y. C.; Tsai, M. H.; Chu, T. C. Using γ-Irradiation to Synthesize Ag Nanoparticles. *Mater. Lett.* **2007**, *61*, 2402−2405.

(9) Gao, H.; Liu, L.; Luo, Y. F.; Jia, D. M. In-Situ Preparation of Epoxy/Silver Nanocomposites by Thermal Decomposition of Silver−Imidazole Complex. *Mater. Lett.* **2011**, *65*, 3529−3532.

(10) Li, X.; He, Y. W.; Ryu, J. S.; Yang, S. I. Colorimetric Detection of Ag Ions with Graphene Oxide in Dimethylformamide. *New J. Chem.* **2014**, *38*, 503−506.

(11) Govorov, A. O.; Richardson, H. H. Generating Heat with Metal Nanoparticles. *Nano Today* **2007**, *2*, 30−38.

(12) Raveendran, P.; Fu, J.; Wallen, S. L. Completely "Green" Synthesis and Stabilization of Metal Nanoparticles. *J. Am. Chem. Soc.* **2003**, *125*, 13940−13941.

(13) Raschip, I. E.; Hitruc, E. G.; Oprea, A. M.; Popescu, M. C.; Vasile, C. In Vitro Evaluation of the Mixed Xanthan/Lignin Hydrogels as Vanillin Carriers. *J. Mol. Struct.* **2011**, *1003*, 67−74.

(14) Pokhrel, D.; Viraraghavan, T. Treatment of Pulp and Paper Mill Wastewater—A Review. *Sci. Total Environ.* **2004**, *333*, 37−58.

(15) Aso, T.; Koda, K.; Kubo, S.; Yamada, T.; Nakajima, I.; Uraki, Y. Preparation of Novel Lignin-Based Cement Dispersants from Isolated Lignins. *J. Wood Chem. Technol.* **2013**, *33*, 286−298.

(16) Adebayo, M. A.; Prola, L. D.; Lima, E. C.; Puchana-Rosero, M.; Cataluña, R.; Saucier, C.; Umpierres, C. S.; Vaghetti, J. C.; Da Silva, L. G.; Ruggiero, R. Adsorption of Procion Blue MX-R Dye from Aqueous Solutions by Lignin Chemically Modified with Aluminium and Manganese. *J. Hazard. Mater.* **2014**, *268*, 43−50.

(17) Khan, M. A.; Ashraf, S. M.; Malhotra, V. P. Development and Characterization of a Wood Adhesive Using Bagasse Lignin. *Int. J. Adhes. Adhes.* **2004**, *24*, 485−493.

(18) Mafongoya, P.; Barak, P.; Reed, J. Carbon, Nitrogen, and Phosphorus Mineralization of Tree Leaves and Manure. *Biol. Fertil. Soils* **2000**, *30*, 298−305.

(19) Cotoruelo, L. M.; Marqués, M. D.; Levia, A.; Rodríguez-Mirasol, J.; Cordero, T. Adsorption of Oxygen-Containing Aromatics Used in Petrochemical, Pharmaceutical, and Food Industries by Means of Lignin-Based Active Carbons. *Adsorption* **2011**, *17*, 539−550.

(20) Sakagami, H.; Kushida, T.; Oizumi, T.; Nakashima, H.; Makino, T. Distribution of Lignin−Carbohydrate Complex in Plant Kingdom

and Its Functionality as Alternative Medicine. *Pharmacol. Ther.* **2010**, *128*, 91−105.
(21) El Mansouri, N. E.; Salvadó, J. Analytical Methods for Determining Functional Groups in Various Technical Lignins. *Ind. Crops Prod.* **2007**, *26*, 116−124.
(22) Liu, B.; Li, X. Y.; Zheng, C. F.; Wang, X. Y.; Sun, R. C. Facile and Green Synthesis of Silver Nanoparticles in Quaternized Carboxymethyl Chitosan Solution. *Nanotechnology* **2013**, *24*, 1−9.
(23) Pan, X. J.; Sano, Y. Fractionation of Wheat Straw by Atmospheric Acetic Acid Process. *Bioresour. Technol.* **2005**, *96*, 1256−1263.
(24) Sun, Y. G.; Xia, Y. N. Shape-Controlled Synthesis of Gold and Silver Nanoparticles. *Science* **2002**, *298*, 2176−2179.
(25) Podsiadlo, P.; Paternel, S.; Rouillard, J. M.; Zhang, Z.; Lee, J.; Lee, J. W.; Gulari, E.; Kotov, N. A. Layer-by-Layer Assembly of Nacre-like Nanostructured Composites with Antimicrobial Properties. *Langmuir* **2005**, *21*, 11915−11921.
(26) Yin, Y.; Li, Z. Y.; Zhong, Z.; Gates, B.; Xia, Y.; Venkateswaran, S. Synthesis and Characterization of Stable Aqueous Dispersions of Silver Nanoparticles Through the Tollens Process. *J. Mater. Chem.* **2002**, *12*, 522−527.
(27) Tran, H. V.; Tran, L. D.; Ba, C. T.; Vu, H. D.; Nguyen, T. N.; Pham, D. G.; Nguyen, P. X. Synthesis, Characterization, Antibacterial, and Antiproliferative Activities of Monodisperse Chitosan-Based Silver Nanoparticles. *Colloids Surf., A* **2010**, *360*, 32−40.
(28) Raghavendra, G. M.; Jayaramudu, T.; Varaprasad, K.; Sadiku, R.; Ray, S. S.; Mohana Raju, K. Cellulose−Polymer−Ag Nanocomposite Fibers for Antibacterial Fabrics/Skin Scaffolds. *Carbohydr. Polym.* **2013**, *93*, 553−560.
(29) Baalousha, M. Aggregation and Disaggregation of Iron Oxide Nanoparticles: Influence of Particle Concentration, pH, and Natural Organic Matter. *Sci. Total Environ.* **2009**, *407*, 2093−2101.
(30) Kundu, S.; Wang, K.; Liang, H. Size-Controlled Synthesis and Self-Assembly of Silver Nanoparticles within a Minute Using Microwave Irradiation. *J. Phys. Chem. C* **2008**, *113*, 134−141.
(31) Nguyen, T. H.; Lee, K. H.; Lee, B. T. Fabrication of Ag Nanoparticles Dispersed in PVA Nanowire Mats by Microwave Irradiation and Electro-Spinning. *Mater. Sci. Eng., C* **2010**, *30*, 944−950.
(32) Zhang, Z.; Xu, F.; Yang, W.; Guo, M.; Wang, X.; Zhang, B.; Tang, J. A Facile One-Pot Method to High-Quality Ag-Graphene Composite Nanosheets for Efficient Surface-Enhanced Raman Scattering. *Chem. Commun.* **2011**, *47*, 6440−6442.
(33) Xiang, Q.; Meng, G.; Zhang, Y.; Xu, J.; Xu, P.; Pan, Q.; Yu, W. Ag Nanoparticle Embedded-ZnO Nanorods Synthesized via a Photochemical Method and its Gas-Sensing Properties. *Sens. Actuators, B* **2010**, *143*, 635−640.
(34) Xu, J.; Chang, Y.; Zhang, Y.; Ma, S.; Qu, Y.; Xu, C. Effect of Silver Ions on the Structure of ZnO and Photocatalytic Performance of Ag/ZnO Composites. *Appl. Surf. Sci.* **2008**, *255*, 1996−1999.
(35) Shah, M. S. A. S.; Nag, M.; Kalagara, T.; Singh, S.; Manorama, S. V. Silver on PEG−PU−$TiO_2$ Polymer Nanocomposite Films: An Excellent System for Antibacterial Applications. *Chem. Mater.* **2008**, *20*, 2455−2460.
(36) Lu, W.; Gao, S.; Wang, J. One-Pot Synthesis of Ag/ZnO Self-Assembled 3D Hollow Microspheres with Enhanced Photocatalytic Performance. *J. Phys. Chem. C* **2008**, *112*, 16792−16800.
(37) Li, M. F.; Sun, S. N.; Xu, F.; Sun, R. C. Microwave-Assisted Organic Acid Extraction of Lignin from Bamboo: Structure and Antioxidant Activity Investigation. *Food Chem.* **2012**, *134*, 1392−1398.
(38) Wen, J. L.; Sun, S. L.; Xue, B. L.; Sun, R. C. Recent Advances in Characterization of Lignin Polymer by Solution-State Nuclear Magnetic Resonance (NMR) Methodology. *Materials* **2013**, *6*, 359−391.
(39) Fu, D.; Farag, S.; Chaouki, J.; Jessop, P. G. Extraction of Phenols from Lignin Microwave-Pyrolysis Oil Using a Switchable Hydrophilicity Solvent. *Bioresour. Technol.* **2014**, *154*, 101−108.
(40) Vanholme, R.; Demedts, B.; Morreel, K.; Ralph, J.; Boerjan, W. Lignin Biosynthesis and Structure. *Plant Physiol.* **2010**, *153*, 895−905.
(41) Terkhi, M. C.; Taleb, F.; Gossart, P.; Semmoud, A.; Addou, A. Fourier Transform Infrared Study of Mercury Interaction with Carboxyl Groups in Humic Acids. *J. Photochem. Photobiol., A* **2008**, *198*, 205−214.
(42) Jiang, X. C.; Xiong, S. X.; Chen, C. Y.; Chen, W. M.; Yu, A. B. Polyol-Thermal Synthesis of Silver Nanowires for $Hg^{2+}$ Sensing Detection. *J. Nanopart. Res.* **2011**, *13*, 5087−5101.
(43) Wu, H. L.; Ji, X. H.; Zhao, L. L.; Yang, S.; Xie, R. G.; Yang, W. S. Shape Evolution of Citrate Capped Gold Nanoparticles in Seeding Approach. *Colloids Surf., A* **2012**, *415*, 174−179.
(44) Yang, Z. S.; Chang, H. T. Anisotropic Syntheses of Boat-Shaped Core-Shell Au-Ag Nanocrystals and Nanowires. *Nanotechnology* **2006**, *17*, 2304−2310.
(45) Vázquez, G.; González-Álvarez, J.; Freire, S.; López-Lorenzo, M.; Antorrena, G. Removal of Cadmium and Mercury Ions from Aqueous Solution by Sorption on Treated *Pinus pinaster* Bark: Kinetics and Isotherms. *Bioresour. Technol.* **2002**, *82*, 247−251.
(46) Chen, X. J.; Zu, Y. B.; Xie, H.; Kemas, A. M.; Gao, Z. Q. Coordination of Mercury(II) to Gold Nanoparticle Associated Nitrotriazole towards Sensitive Colorimetric Detection of Mercuric Ion with a Tunable Dynamic Range. *Analyst (Cambridge, U.K.)* **2011**, *136*, 1690−1696.